Materials Advances

ROYAL SOCIETY OF CHEMISTRY

PAPER

View Article Online
View Journal | View Issue

Cite this: *Mater. Adv.*, 2025, **6**, 7837

Clay-based polyurethane foam nanocomposites for thermal insulation

Tomonori Watanabe,†[a] Haruna Sasaki,†[a] Yuhei Nakashima,[b] Nobuyoshi Miyamoto,[cd] Hideki Takamura,[e] Kunihiro Nakano[c] and Tomohiko Okada †*[a]

Received 18th June 2025,
Accepted 6th September 2025

DOI: 10.1039/d5ma00651a

rsc.li/materials-advances

9wPolyurethane foams are classes of cellular plastics that exhibit mechanical robustness and lightness; they are widely applied as thermal insulators in the building and automotive fields. Nanocomposites play an important role in improving the energy efficiency of thermal insulation materials. In this study, a layered clay mineral (montmorillonite) was used as a nanosheet-type gas-barrier filler in a foam-type urethane/urea/isocyanurate copolymer to delay exchanges of thermal insulation gases (carbon dioxide and 1,3,3,3-tetrafluoropropene) in the polyurethane foam with air. This gas barrier is expected to prevent the deterioration of its long-term thermal insulation performance. Synchrotron radiation small-angle X-ray scattering was used to analyze the dispersion of the clay nanosheets modified with organic cations in the polyurethane matrix. The cations include benzyldimethylhexadecylammonium (C_{16}2MeB), dimethyldioleylammonium (2$C_{18=}$2Me), and bis(2-hydroxyethyl)dimethylammonium (2EtOH2Me). The 2EtOH2Me-clay adduct was highly dispersed in the polymeric matrix, possibly because of its good compatibility with a polyurea domain. The dense ordering of C_{16}2MeB-clay in the polymeric matrix influenced the degradation of its thermal insulation performance. The degree of ordering in the polymeric matrix was reduced by decreasing the layer charge density of the negative charge in the montmorillonite, thereby improving the insulation performance for 4 months empirically. The reduction of the effects on power consumption during heating was simulated using a detached house over 30 years. This study designed a gas barrier agent for the macropore wall of PU foam.

Introduction

Polyurethane (PU) contains urethane/urea groups in its main skeleton. Depending on the starting components, PU has been fabricated as products ranging from soft flexible urethane foams to durable rigid urethane foams, films, fibers, and molded devices. Thermal insulation materials using rigid urethane foams are in high demand as residential building materials due to their durability, low thermal conductivity, and on-site producibility, which help in preventing global warming and reducing resource consumption by lowering energy consumption for heating/cooling.[1] Considering that the lifespan of a house is several tens of years, insulation materials with low thermal conductivity are desired because of their minimal deterioration in insulation over a long period. Rigid urethane foam exhibits high thermal insulation by retaining gas with low thermal conductivity in its closed macropores. However, the insulating gas diffuses from the pores and is replaced with air, thereby lowering the insulation performance. Nanosheets are promising candidates for gas barrier agents in the thin gas cell wall of PU foam for effectively sealing the insulating gas to improve the long-term stability of the insulation performance.

The established production of PU foam can be divided into two steps.[2] In the first step, a premix liquid is prepared by mixing polyols (POs) with functional additives, such as surfactants,[3] flame retardants, blowing agents, and catalysts. In the second step, isocyanate (as a cross-linking agent) and a gas with low thermal conductivity liquefied at a low temperature (as a physical blowing agent) are added to the premix. Fig. 1 shows that isocyanate (polymeric methylene diphenyl diisocyanate (MDI)) and the POs react to form a urethane group, and a simultaneous reaction of the isocyanate with H_2O forms a urea group. Additionally, a part of the isocyanate undergoes a trimerization reaction to form an isocyanurate group.

The heat of the polymerization reaction initiates foaming, trapping the insulating gas in the closed pores. When the pores

[a] *Department of Materials Chemistry, Faculty of Engineering, Shinshu University, 4-17-1 Wakasato, Nagano, 380-8553, Japan. E-mail: tomohiko@shinshu-u.ac.jp*
[b] *Tosoh Corporation Ltd, 2743-1 Hayakawa, Ayase, Kanagawa, 252-1123, Japan*
[c] *Department of Life, Environment and Applied Chemistry, Graduate School of Engineering, Fukuoka Institute of Technology, Fukuoka, 3-30-1 Wajiro Higashi, Higashi-ku, Fukuoka, 811-0295, Japan*
[d] *International Institute for Sustainability with Knotted Chiral Meta Matter, Hiroshima University, Higashi-hiroshima, Japan*
[e] *Department of Architecture, Faculty of Engineering, Shinshu University, 4-17-1 Wakasato, Nagano, Nagano, 380-8553, Japan*
† T. O., T. W., and H. S. contributed equally to this work.

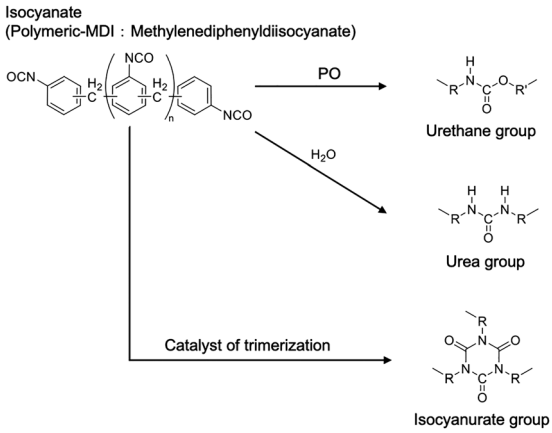

Fig. 1 Polymerization process of the urethane/urea/isocyanurate copolymer.

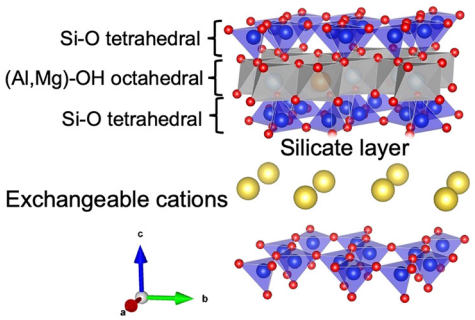

Fig. 2 Structure of montmorillonite comprising nanometer-thick crystalline silicate layers (two tetrahedral sheets and an octahedral sheet; 2 : 1 type) and interlayer cations.

become sufficiently small to approach the mean free path of the gas, there is a higher probability of the gas molecules colliding with the pore wall than with each other to prevent heat exchange.[4] The addition of microparticles and nanoparticles into PU foams has been reported with the expectation for such PU foams to be effective as flame retardants, foam stabilizers, and gas-barrier agents. During the foaming process, these particles function as bubble-generation nuclei to reduce the size of the macropores.[5] Silica,[6,7] clays,[8,9] cellulose,[10] lignin,[11] and biomass-derived ash[12] are representative substances for improving thermal insulation.[13,14] In addition to the Knudsen effect, lowering the gas permeability of the PU phase is important for avoiding deterioration in the thermal insulation performance. Typical POs are polymers with a low molecular weight, such as polyethers and polyesters with two or more hydroxyl groups at their end groups. A polymer with a low molecular weight causes microphase separation between the polyether/polyester and PU/polyurea phases,[8] which improves the flexibility of PU foam. However, in the case of a negligible contribution of the crystalline PU/polyurea layer to gas permeation, the glassy polyether/polyester phase undergoes slight thermal movement, leaking the low thermal conductivity gas through fine pores at the molecular level. Thus, dispersing a gas-barrier agent in the glassy phase is a prerequisite for gas sealing.[15,16]

Here, a layered clay mineral was used as a gas-barrier agent. Layered clay minerals have been applied as fillers to drastically improve polymer performance, even when only a low mass percent of the mineral is added to the polymer. This is exemplified in the pioneering study on nylon-clay nanocomposites using montmorillonite (Mnt).[17–19] Mnt is a swellable layered inorganic solid comprising approximately a 1-nm-thick silicate layer in which an octahedral sheet is sandwiched between tetrahedral sheets (Fig. 2).[20] When PU is adsorbed between the silicate layers of Mnt, the interlayer space may expand and/or exfoliate.[21] Owing to the ultrathin silicate layer and the large lateral plate-like structure (tens of nanometers to several micrometers),[22] the highly dispersed silicate layer with a high aspect ratio frequently causes a labyrinth effect.[23] This effect acts as an obstacle in the gas permeation path in the polymer matrix. A mixed phase of exfoliated and intercalated structures is more common than the homogeneous exfoliated structure; the silicate layer is uniformly dispersed as secondary particles with a laminated structure of several layers.[24]

Part of the trivalent Al ions in the octahedral sheet of Mnt are apparently replaced by divalent Mg ions (isomorphous substitution) and/or form defects (vacancies).[25,26] Thus, the silicate layers are superimposed by hydrated exchangeable cations (*e.g.*, Na and Ca) to compensate for a permanent negative charge (Fig. 2). Mnt becomes hydrophobic when the exchangeable cations are replaced with an organic cation, such as a long-chain alkylammonium ion.[27–30] Organic cations reduce the surface polarity of the silicate layer; thus, affinity with the polymer matrix is expected to be enhanced.[31,32] However, if the electrostatic interactions between the silicate layer and interlayer cations are strong, exfoliation would be difficult. Thus, the organic cations to be modified and the layer charge density of Mnt determine the exfoliation in the skeleton of PU foams.

This study discusses the dispersibility (exfoliated/laminated structure) of Mnt in PU foam by changing the functionality of organic cations and the layer charge density of Mnt controlled by Li-charge reduction (Hofmann–Klemen effect[33]). Li-charge reduction has been employed as a method for reducing layer charge density by Li^+ fixation into the framework of the silicate layers of Mnt to neutralize the negative layer charge through the heat treatment of Li-saturated Mnt. The layer charge density decreases with the heating temperature because a large amount of Li^+ migrates toward the vacancy in the octahedral sheet. The Li-reduced charge Mnt (RCM) is vital for optimal dispersibility in solvents and polymers for certain adsorbent[34,35] and polymer filler applications,[36–40] owing to weak electrostatic cation–silicate interactions. According to a study based on ^{7}Li-NMR analyses, the penetration depth of Li ions varies with the heating temperature.[41] However, the Li^+ distribution in RCM is quantitatively unclear at present but may be broad. When a mixture of alcohol and an aqueous ammonia solution was added to an aqueous dispersion of RCM, the dispersibility of RCM increased.[42,43] Although the mechanism for enhancing dispersibility remains unclear, the alcohol and ammonia may

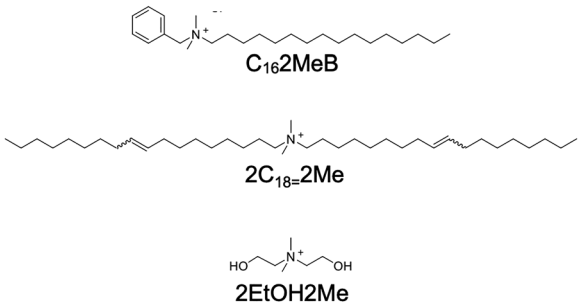

Scheme 1 Molecular structures of C_{16}2MeB, 2$C_{18=}$2Me, and 2EtOH2Me cations.

selectively eliminate Li ions which are not located in the octahedral vacancy (*e.g.*, vicinity of the tetrahedral sheet). This could result in uniform charge distribution and moderate/intermediate layer charge density. Three types of cations have been used (Scheme 1) to obtain organically modified Mnt. Two of them exhibit low polarity. They include benzyldimethylhexadecylammonium (C_{16}2MeB) and dimethyldioleylammonium (2$C_{18=}$2Me), which bear benzyl and olefin groups, respectively. The third cation, bis(2-hydroxyethyl)dimethylammonium (2EtOH2Me), exhibits high polarity owing to a hydroxyl group. Here, we provide a reasonable design of a gas-barrier agent for the macropore wall of PU foam using RCM and the aforementioned organic cations through analyses, including ultrasmall-angle synchrotron X-ray scattering measurements.

Experimental section

Reagents and materials

Na–Mnt (Kunipia F, JCSS–3101; $(Na_{0.53}Ca_{0.09})^{0.71+}([Al_{3.28}Fe_{0.31}Mg_{0.43}][Si_{7.65}Al_{0.35}]O_{20}(OH)_4)^{0.71-}$), a reference clay sample from the Clay Science Society of Japan, was supplied by Kunimine Industries Co., Ltd (Tokyo, Japan). The cation exchange capacity (CEC) of Kunipia F is 1.19 meq g^{-1} clay.[44] Li ion exchanged–Mnt (Kunipia M) was supplied by Kunimine Ind. Co., Ltd (Tokyo, Japan).

Benzyldimethylhexadecylammonium chloride (C_{16}2MeB–Cl, Sigma-Aldrich Chemical Co., Inc., St. Louis, MO, USA), dimethyldioleylammonium chloride (2$C_{18=}$2Me–Cl, Lion Specialty Chemical Co., Ltd, Tokyo, Japan), and bis(2-hydroxyethyl)dimethylammonium chloride (2EtOH2Me–Cl, Tokyo Chemical Industry Co., Ltd, Tokyo, Japan) were purchased and used as received. Ammonium hydroxide (28% in water) and dimethyldioctadecylammonium bromide (2C_{18}2Me–Br) were purchased from FUJIFILM Wako Pure Chemical Co., Ltd (Osaka, Japan).

Low molecular weight POs (MAXIMOL, RFK-556 and RFK-505) were purchased from Kawasaki Kasei Chemicals Ltd (Kanagawa, Japan). Tris(chloropropyl)phosphate was purchased from Daihachi Chemical Industry Co., Ltd (Osaka, Japan). Octamethylcyclotetrasiloxane (Niax™ silicone L-6078) was purchased from Momentive Performance Materials Japan LLC (Tokyo, Japan). A mixture of 1,2-dimethylimidazole and ethane-1,2-diol (TOYOCAT-DM70) and a mixture of a quaternary ammonium salt and ethylene glycol (TOYOCAT-TRX) were supplied by Tosoh Corp. (Tokyo, Japan). Polymeric MDI (MR-200) was used as isocyanate (Tosoh Corp.). Hydrofluoroolefin (HFO-1233zd, 1,3,3,3-tetrafluoropropene) was obtained from Central Glass Co., Ltd.

Preparation of reduced charge montmorillonite

The Li^+-exchanged montmorillonite (50 g) was sequentially heat-treated at 110 °C for 1 h and then heated at 235 °C for 1.5 h in air. The heat-treated powder is denoted hereinafter as RCM. After immersing the RCM (0.5 g) in a water/ethanol (50/50 = v/v) mixture (10 mL), an aqueous ammonia solution (28%, 0.5 mL) was stirred magnetically for 1 h at room temperature to provide a slurry. The solid component in this slurry is denoted hereinafter as RCM–NH_3. Ion exchange reactions of RCM, RCM–NH_3, and Na–Mnt were examined using 2C_{18}2Me–Br to determine the CEC.[45,46] For the RCM–NH_3, the resulting slurry was allowed to react with 2C_{18}2Me–Br (0.50 mmol) dissolved in a mixture of water/ethanol (50/50 = v/v) at 70 °C for 24 h. To determine the CECs of RCM and Na–Mnt, their powders (0.5 g) were immersed into a water/ethanol (50/50 = v/v) mixture (10 mL) and allowed to react with 2C_{18}2Me–Br (0.50 and 0.65 mmol, respectively) at 70 °C for 24 h. These precipitated ion exchange adducts were repeatedly washed with water and ethanol, until a negative test for Cl^- or Br^- was obtained using $AgNO_3$. After drying at 50 °C overnight, powder X-ray diffraction (XRD) analysis was performed using a Rigaku MiniFlex 600 diffractometer to measure the basal spacing (d_{001}). The powder XRD measurements (with monochromatic Cu Kα irradiation) were conducted at 15 mA and 40 kV within a 2θ range of 3°–30°, and the sampling step and the scanning rate were 0.02° and 2° per min, respectively. The amount of adsorbed 2C_{18}2Me cations was determined *via* thermogravimetric–differential thermal analysis (TG–DTA) curves recorded in air using a Rigaku TG8120 instrument at a heating rate of 10 °C min^{-1}, with α-alumina as the standard material.

Preparation of organically modified Mnt

C_{16}2MeB-, 2$C_{18=}$2Me-, and 2EtOH2Me-modified Mnt samples were prepared through the ion exchange reactions of Na–Mnt. The loaded amount of the organoammonium chloride was 0.65 mmol *versus* Na–Mnt (0.5 g) in each sample. The solvent (10 mL) used in the reaction was water for 2$C_{18=}$2Me–Cl and 2EtOH2Me–Cl, whereas a water/ethanol (50/50 = v/v) mixture was used for C_{16}2MeB–Cl. The Na–Mnt mixture was magnetically stirred for 24 h at room temperature. C_{16}2MeB–RCM was prepared under the same conditions, except that the amount of loaded C_{16}2MeB–Cl was reduced to 0.50 mmol. C_{16}2MeB–RCM–NH_3 was prepared by mixing a slurry comprising RCM (0.5 g), a water/ethanol mixture (10 mL), and an ammonia solution (28%, 0.5 mL) with C_{16}2MeB–Cl (0.50 mmol) in a water/ethanol (50/50 = v/v) mixture through magnetic stirring for 24 h. The obtained precipitates were repeatedly washed with the solvent used for the ion exchange reactions, until a negative test for Cl^- was obtained. After drying at 50 °C overnight, powder XRD and TG–DTA were performed.

Preparation of polyurethane foam

After drying the organically modified Mnt in air at 80 °C overnight, POs (mixed liquid of RFK-556 and RFK-505) were mixed at 70 °C using a wind turbine blade-type mechanical homogenizer under shaking at 3500 rpm for 30 min. The resulting PO suspension was mixed with a premix solution, which had the chemical composition of the reagents listed in the SI, under shaking using the same homogenizer at 1200 rpm for 30 min at room temperature. Finally, isocyanate and 1,3,3,3-tetrafluoropropene were added to the resulting mixture under shaking at 5000 rpm for 3 s, and the mixture was immediately poured into a mold to form PU foam. As a control experiment, no-clay PU foam was prepared using the same procedure.

The PO suspension was analyzed using another XRD apparatus (a Rigaku SmartLab diffractometer) by recording under monochromatic Cu Kα irradiation at 30 mA and 40 kV within a 2θ range of 0.5°–8°. The sampling step and the scanning rate were 0.02° and 2° per min, respectively. Structural analyses in the premix solution were conducted by small-angle X-ray scattering (SAXS) using a Rigaku NANOPIX (monochromatic Cu Kα irradiation at 30 mA and 40 kV). The camera distances were 714.26 mm ($0.06 < q < 0.6$ nm^{-1}) and 216.3 mm ($q > 0.6$ nm^{-1}). During these analyses, the samples were introduced into a thin glass capillary (ϕ = 0.7 mm). The SAXS patterns were recorded by subtracting the premix solution from the mixture of the premix with the clay-PO suspension.

The structural analyses of the PU foams were performed using a synchrotron radiation SAXS measurement system developed at the BL19B2 beamline facility in SPring-8. The camera distances were 3 and 41 m for the radiation of 18-keV synchrotron X-rays when measuring within the q ranges of 0.06–1 and 0.003–0.1 nm^{-1}, respectively. Crushed PU foams were introduced into a thin quartz glass capillary (ϕ = 2.0 mm). Photographs of the crushed PU samples were obtained using a polarized light microscope (Olympus BX 51). The thermal conductivity was recorded using an EKO FOX314/HC074 tester.

Calculation of reducing CO_2 emission in a detached house using a PU foam hybrid

Power consumption in heating over 30 years was calculated to evaluate the energy-saving performance in a detached house model. A typical wooden two-story building was used as a detached house model (total floor area = 142 m^2, Fig. S1). All of the outer skin (*e.g.*, outer wall, floor, and roof) in the building was embedded with a rigid PU foam (with a thickness of 50 mm), where the volumetric specific heat is 60 kJ m^{-3} K^{-1}. The specific heat loss [W m^{-2} K^{-1}] was obtained by transferring heat from the interior space to the outside through the outer skin, according to the Homes-kun (INTEGRAL Corp., Tsukuba, Japan) software. The 1-year power consumption [kWh] within a heating period (from October 24th to May 1st in Nagano City) was calculated using the simulated thermal conductivity at 30 years (the time-course difference is shown in the SI) and the heating load (Homes-kun software) at a constant indoor temperature (293 K). Finally, the total CO_2 emission [kg-CO_2] during heating for 30 years was determined by multiplying the CO_2-emission coefficient (0.459 kg-CO_2 kWh^{-1}) by the thirty-fold power consumption.

Results and discussion

Organic modification of Mnt

The amounts of the organic cations exchanged into Na-Mnt were measured using thermal analyses (Table 1; the TG–DTA curves are shown in Fig. S2). The amounts of C_{16}2Me, 2$C_{18=}$2Me, and 2EtOH2Me cations were 1.1, 1.2, and 1.0 meq g^{-1}, respectively (Table 1). Considering the CEC of Na–Mnt (1.19 meq g^{-1}), quantitative ion exchange was confirmed between the organic and interlayer cations (*e.g.*, Na^+ and Ca^{2+}) in Na–Mnt. The powder XRD patterns of the resulting ion exchange adducts (organically modified Mnt) shown in Fig. 3 revealed interlayer expansion (intercalation) upon ion exchanges. The basal spacings of C_{16}2Me–, 2$C_{18=}$2Me–, and 2EtOH2Me–Mnt increased to 2.0, 3.0, and 1.4 nm, respectively (Table 1), from that (1.2 nm) of Na–Mnt. This corresponded to the interlayer spaces of 1.0, 2.0, and 0.4 nm, respectively, obtained by subtracting the thickness of the silicate layer (1.0 nm) from the observed basal spacings. The number of alkyl chains in the organic cations and/or molecular geometry influenced the basal spacing. The cationic head groups in the C_{16}2MeB[47,48] and 2$C_{18=}$2Me[49] cations were considered to be anchored to the basal plane of the silicate layer with their alkyl chains inclining at a tilt angle. It has been reported that the C=C double bond in 2$C_{18=}$2Me undergoes a *gauche* conformation with a lower packing as the 2$C_{18=}$2Me assembly in the interlayer space.[49] In contrast, the interlayer distance (0.4 nm) of 2EtOH2Me–Mnt corresponded to the monomolecular layer of 2EtOH2Me with a

Table 1 Cation exchange capacity (CEC) of the host, adsorbed amount of organic cations, and basal spacing of the organically modified samples prior to and after the immersion of PO

Sample	CEC[a]/mmol g^{-1}	Amount of adsorbed organic cations/mmol g^{-1}	Basal spacing/nm	
			Prior to PO immersion	After PO immersion
C_{16}2MeB–Mnt	1.19	1.1	2.0	3.7
C_{16}2MeB–RCM–NH_3	0.52	0.51	1.5	1.5
C_{16}2MeB–RCM	0.29	0.21	1.4	1.4
2$C_{18=}$2Me–Mnt	1.19	1.2	3.0	3.7
2EtOH2Me–Mnt	1.19	1.0	1.4	1.4

[a] Determined by the amount of adsorbed 2C_{18}2Me cations.

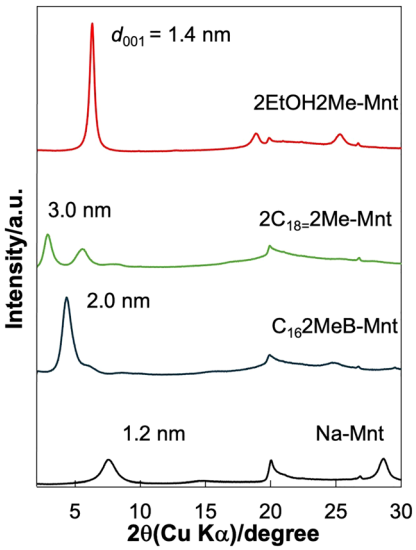

Fig. 3 Powder XRD patterns of Na–Mnt and the organically modified Mnt samples.

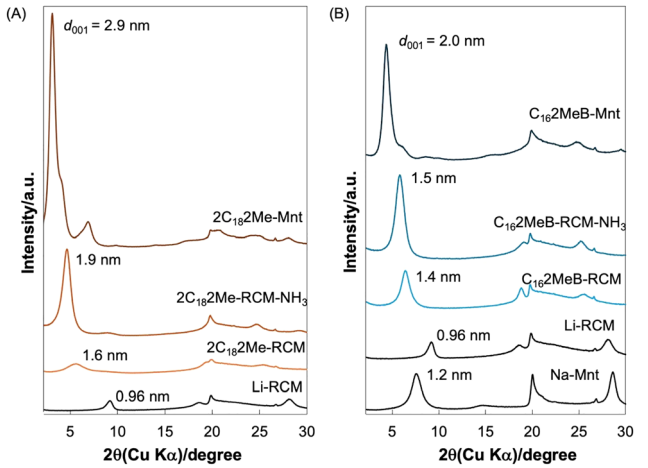

Fig. 4 Powder XRD patterns of (A) $2C_{18}$2Me- and (B) C_{16}2MeB-adducts using montmorillonites with different layer charge densities (CECs).

void nanospace in the interlayers, called pillared or microporous clays.

Reducing layer charge density

Ion exchange with dimethyldioctadecylammonium ($2C_{18}$2Me) was employed to determine the CEC because it directly correlates with the layer charge density.[45,46] A series of *n*-alkylammonium ions has been used in the ion exchange to estimate the layer charge density and internal surface areas of cation-exchangeable layered materials.[50,51] The basal spacing (interlayer space of Mnt) increases stepwise as a function of the chain length of intercalated *n*-alkylammonium ions, suggesting a transition of the molecular arrangement from monomolecular to pseudo-trimolecular *via* bimolecular layers. Quaternary alkylammonium has been used to determine the internal surface area of smectites.[52] As shown in the powder XRD patterns (Fig. 4A), the basal spacings of the $2C_{18}$2Me-adducts were 1.6 (bilayer), 1.9 (pseudo-trimolecular), and 2.9 nm (paraffin type),[44] when RCM, RCM–NH_3, and Na–Mnt were used as host materials, respectively. Owing to the large molecular size of $2C_{18}$2Me ions, a paraffin-type arrangement in the interlayer space is plausible, when the Mnt sample with a large CEC (1.19 meq g^{-1}) was used.[44] The amount of adsorbed $2C_{18}$2Me cations on Na–Mnt (Table 1) was consistent with the CEC determined using thermal analysis, and the TG–DTA curves are shown in Fig. S3. The same procedure was applied to RCM and RCM–NH_3, resulting in CECs of 0.29 and 0.52 meq g^{-1}, respectively.

The organic modification of the RCM was performed to prepare gas-barrier agents for PU using C_{16}2MeB cations. The adsorbed amounts of C_{16}2MeB cations were 0.21 on RCM and 0.51 meq g^{-1} on RCM–NH_3 (determined using thermal analyses, Fig. S2) and were close to the CECs, revealing the replacement of Li^+ with C_{16}2MeB cations. The cation exchange caused an increase in the basal spacing from 0.96 nm (RCM, the dehydrated Li^+-exchanged form) to 1.4 and 1.5 nm for RCM and RCM–NH_3, respectively (Fig. 4B). The resulting smaller d_{001} values than that (2.0 nm) in C_{16}2MeB–Mnt indicate that the head group of C_{16}2MeB would anchor and incline at a lower tilt angle.

Intercalation of PO

Prior to the polymerization of the low molecular weight PO to PU, the affinity of organically modified Mnt samples with PO was examined. Powder XRD patterns were recorded (Fig. 5) after mixing five types of organically modified Mnt samples (0.15 g) with the PO (9.85 g). The interlayer spaces of C_{16}2MeB–Mnt and $2C_{18=}$2Me–Mnt (CEC = 1.19 meq g^{-1}) expanded to d_{001} = 3.7 nm upon the intercalation of PO. However, a slight increase in the d_{001} was observed for the other samples. No peak in the d_{001} range of 2–4 nm was observed, indicating a nonreacted phase (d = 1.5 nm) rather than the delamination of stacked layers by

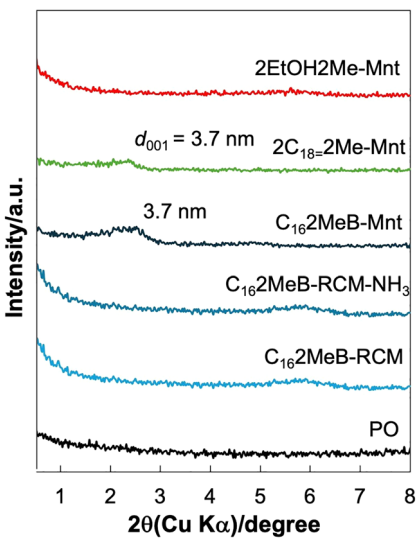

Fig. 5 Powder XRD patterns of the PO mixtures with organically modified montmorillonites.

the uptake of a large amount of PO. The poor intercalation characteristics of PO can be explained in terms of a low CEC and the high polarity of the organic cations.

The layer charge density (CEC) is expected to influence the swelling ability in the PO, premix solution (including water), and dispersion in the final PU foams. When the CEC of Mnt is large, the swelling ability of Mnt is restricted because of strong electrostatic interactions.[53] The restriction of the swelling ability was relieved within the CEC range of 0.6–1.5 meq g^{-1}. In contrast, an RCM within the aforementioned range has been reported to exhibit a large capacity for the uptake of an organic molecule in water.[35] The CEC was reduced by decreasing the interlayer hydrated Li^+, namely, an increase in the amount of Li^+ fixed into the Mnt framework through heat treatment for a long period and at a high temperature.[55] The reduction in the CEC to less than 0.6 meq g^{-1} lowered the hydrophilicity[40,55] and the uptake of an organic molecule into the organically modified RCMs.[39] In the present PO intercalation test, no swelling was observed in C_{16}2MeB–RCM–NH_3 (CEC = 0.52 meq g^{-1}) and C_{16}2MeB–RCM (CEC = 0.29 meq g^{-1}).

The heat treatment of Li^+-exchanged Mnt (Kunipia M) at 235 °C for 1.5 h diminished the CEC from 1.19 to 0.29 meq g^{-1}, according to the aforementioned adsorption test of 2C_{18}2Me cations on the RCM. Reactions of ammonia with RCM regulated the layer charge density to a moderate level in RCM–NH_3 (CEC = 0.52 meq g^{-1}). The increase in the layer charge density of RCM can be explained in terms of eliminating the dehydrated Li^+ at a specific position from the RCM framework. The location of Li^+ in the RCM framework remains controversial, whether in the vacancy of the octahedral sheet or far from the vacancy. According to Hofmann and Klemen,[33] the location of fixed Li ions is the octahedral sheet (Fig. 1 and 6). Decarreau *et al.* pointed out that lattice defects in an octahedral AlO_6 gibbsite sheet (or MgO_6 brucite sheet) of Mnt are the origin of negative charges.[25] It is thought that dehydrated Li ions are fixed to these lattice defects to neutralize the negative charges (migration from positions 1 to 4 in Fig. 6). Li ions penetrate the lattice defects of the octahedral sheet and the vicinity of the SiO_4 tetrahedral sheet.[41] A large quantity of hydrated Li ions possibly migrated at a higher heating temperature toward the lattice defects in the octahedral sheet, but dehydration was fixed on the path of the vacancy. This is schematically exemplified in positions 2 and 3 in Fig. 6 at the hexagonal hole and hydroxyl groups of an AlO_6 gibbsite sheet (or a MgO_6 brucite sheet), respectively.

Dehydrated Li ions have been reported to be fixed in the vicinity of the SiO_4 tetrahedral sheet.[54] Thus, we hypothesize that Li^+ fixation on hydroxyl groups stuck out of the octahedral $M_{oct}O_4(OH)_2$ sheet (M_{oct} = Al^{3+} or Mg^{2+} at position 3). In addition, $Li^+OH^{\delta-}$–$M_{oct}{}^{\delta+}$ would function as a base in the aqueous mixture of a halide (*e.g.*, Cl^- and Br^-) and $NH_4{}^+$ to liberate NH_3. Ammonia hydrolysis afforded $NH_4{}^+$ to react with the organoammonium salts (*e.g.*, C_{16}2MeB–Cl and 2C_{18}2Me–Br), followed by the liberation of NH_3 upon reactions with $Li^+OH^{\delta-}$–$M_{oct}{}^{\delta+}$. The standard reaction Gibbs energy for the reaction between a weak base salt (*e.g.*, NH_4Br) and a strong base (LiOH) was calculated to be a negative value between –20 and –30 kJ mol^{-1}. This calculation is available in the SI. The base liberation would simultaneously cause the rehydration of Li^+ at position 3 in the RCM to participate in ion exchange (or increase the layer charge). Importantly, electrostatic interactions would weaken because of the remaining Li^+ in the vacancy (position 4) that is far from the interlayer space (position 1). This is a possible explanation of how weak electrostatic cation–silicate interactions contribute to the good dispersion in PU foam.

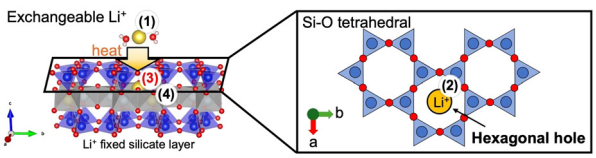

Fig. 6 Illustration of speculative locations of Li ions in a silicate layer of Li^+-exchanged montmorillonite.

Thermal insulation of clay-loaded PU foams

Fig. 7 shows the time-course difference in the thermal conductivity (Δk) for the PU sample without a filler (k_{wof}) and the Mnt-loaded PU (k_f), which can be calculated using eqn (1):

$$\Delta k = k_{wof} - k_f. \quad (1)$$

Irrespective of the presence of fillers, only a negligible difference was observed in the initial thermal conductivities (18.2 mW m^{-1} K^{-1} at 0 day; the original profile is shown in Fig. S4). This indicated that the cell size of the PU foam was scarcely influenced by loading organically modified Mnt. The negative Δk value for C_{16}2MeB–Mnt (CEC = 1.19 meq g^{-1}) implied a degradation in the thermal insulation of PU. An improvement in the insulation (positive value of Δk) was observed when Mnt with a low layer charge density was used. The thermal conductivity at 100 days (Table 2) was in the order

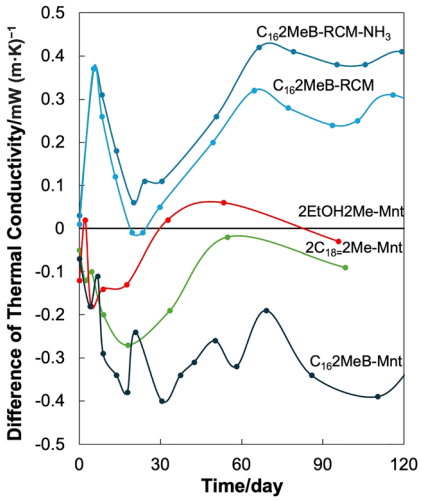

Fig. 7 Time-course profiles of the difference in the thermal conductivity (Δk) of polyurethane (PU) foam (k_{wof}) and organically modified montmorillonite-loaded PU foam (k_f).

Table 2 Cation exchange capacity (CEC) of the host, difference in the thermal conductivity of the no-filler polyurethane recorded at 100 days, and the slope of the power law relationship $I(q) \propto q^{-n}$ in the synchrotron radiation small-angle X-ray scattering measurements shown in Fig. 8

Sample	CEC[a]/ mmol g^{-1}	Δk[b] at 100 days/ mW (m K)$^{-1}$	q^{-n}
C_{16}2MeB–Mnt	1.19	−0.38	3.68
C_{16}2MeB–RCM–NH_3	0.52	+0.38	3.76
C_{16}2MeB–RCM	0.29	+0.26	3.81
$2C_{18=}$2Me–Mnt	1.19	−0.07	3.82
2EtOH2Me–Mnt	1.19	−0.02	3.61

[a] Determined by the amount of adsorbed $2C_{18}$2Me cations. [b] Obtained by subtracting the thermal conductivity of the Mnt-loaded PU (k_f) from that without a filler (k_{wof}).

of C_{16}2MeB–RCM–NH_3 (CEC = 0.52 meq g^{-1}) > C_{16}2MeB–RCM (CEC = 0.29 meq g^{-1}) > C_{16}2MeB–Mnt (CEC = 1.19 meq g^{-1}). In contrast, $2C_{18=}$2Me–Mnt and 2EtOH2Me–Mnt (CEC = 1.19 meq g^{-1}) exhibited minimal improvements.

Synchrotron radiation small-angle X-ray scattering analyses of polyurethane foams

The thermal insulation gases were occluded into macropores (10^2–10^4 μm in size) surrounding a thin PU wall with a thickness ranging from submicrometers to several micrometers. Fig. S5 shows the SEM image. When the silicate layers were loaded into the PU wall, the inner morphology (*e.g.*, cell size and wall thickness) remained almost unchanged owing to the optimized chemical composition of the premix solution (SI). Synchrotron radiation SAXS (SR-SAXS) was employed to detect the degree of ordering of the silicate layers in the resulting clay-loaded PU foams. The SR-SAXS patterns (Fig. 8A) of the clay-loaded PU foams were obtained by subtracting the intensity of the non-clay PU foam from that of the as-recorded clay-loaded foams within a range of $0.06 < q < 3.0$ nm^{-1}. All of the PU foams exhibited a power law relationship, $I(q) \propto q^{-4}$, in a wide-angle range ($0.06 < q < 3.0$ nm^{-1}, right part of Fig. 8A). $I(q)$ and q are the scattering intensity and magnitude of the scattering vector, which is ascribed to the form factor scattering from an isotropic structure (*e.g.*, spherical aggregates of silicates and spherical crystalline domains in PU), respectively. Within the range of $0.06 < q < 3.0$ nm^{-1} (right part of Fig. 8A), a specific peak only appeared for C_{16}2MeB–Mnt (CEC = 1.19 meq g^{-1}) around $q = 0.8$ nm^{-1}. The corresponding d of 4.5 nm ($d = 2\pi/q$) indicates a dense ordered structure in the PU foam due to strong electrostatic interactions and a relatively low compatibility with C_{16}2MeB–PU. The dense ordering is possibly responsible for the deterioration in the long-term thermal insulation performance because of a reduction in the thermal insulation gases based on the tortuous path model.[56] Furthermore, the ordering was reduced when the 2EtOH2Me and $2C_{18=}$2Me cations were used to modify Mnt. Additionally, less ordering was observed for the RCM (CEC = 0.29 meq g^{-1}) and C_{16}2MeB–RCM–NH_3 (CEC = 0.52 meq g^{-1}).

Next, the slope of the power law relationship, $I(q) \propto q^{-n}$, was compared within a small-angle range ($0.06 < q < 0.2$ nm^{-1})

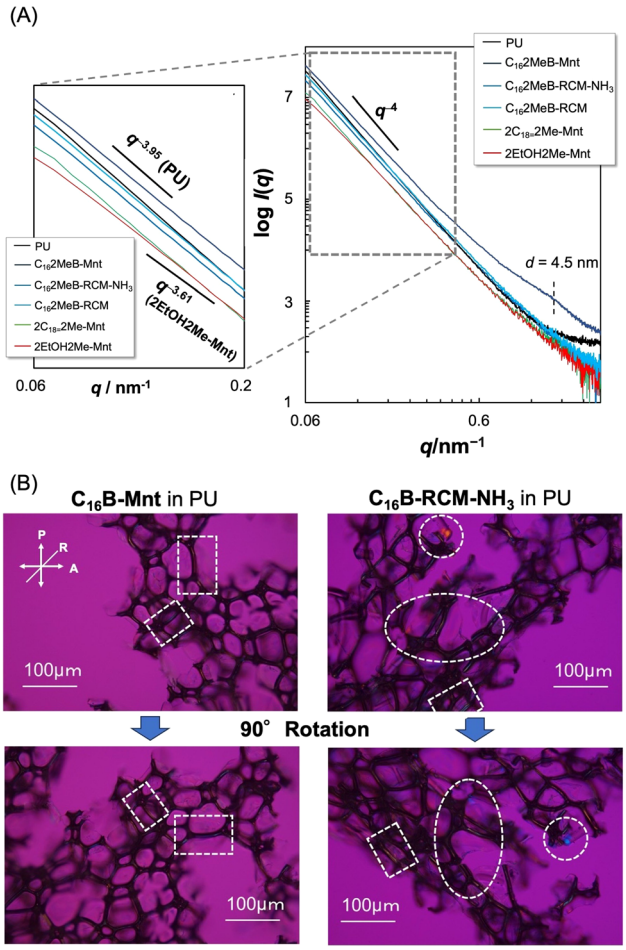

Fig. 8 (A) SR-SAXS patterns of clay-loaded PU foams recorded in (left) small ($0.06 < q < 0.2$ nm^{-1}) and (right) wide ($0.06 < q < 3.0$ nm^{-1}) angle ranges. (B) Typical photographs under crossed polarizers for C_{16}2MeB–Mnt and C_{16}2MeB–RCM–NH_3. The dotted circles and squares indicate dispersion in a thinner cell and aggregates in the cell wall, respectively.

(Table 2). SAXS profiles in a double-component system are mainly obtained from nanosheet scattering because the scattering capability of inorganic nanosheets is more than one order of magnitude higher than that of organic polymers.[57] The profile with a slope of q^{-2} indicates form factor scattering from nanosheets larger than 100 nm in the q range.[58] The particle size of Mnt has been reported to fall within the range of 300–500 nm,[59] and nonuniform aggregates have been indicated to have sizes ranging from over 1 μm for Na–Mnt[60] to approximately 8 μm for organo-Mnt.[61] The slope of q^{-n} for the non-clay PU (−3.95) close to −4 indicated scattering from random aggregates (*e.g.*, an interface between air and PU, crystalline PU domains). However, the absolute n value decreased (3.61–3.81, Table 2) in the presence of Mnt nanosheets in the PU foams. This decrease was caused by the forming mixture of Mnt nanosheets and random aggregates.

The proportion of nanosheets to random aggregates (q^{-2}/q^{-4}) was reflected by the organic cations and CEC of Mnt. The proportion in the C_{16}2MeB–Mnt system decreased in the order of C_{16}2MeB–Mnt (3.68, CEC = 1.19 meq g^{-1}) > C_{16}2MeB–RCM–NH_3

(3.76, CEC = 0.52 meq g^{-1}) > C_{16}2MeB–RCM (3.81, CEC = 0.29 meq g^{-1}). This order indicates that diminishing nanosheets form random aggregates in the PU foams with a decrease in CEC. Typical photographs of PU foams (Fig. 8B) under crossed polarizers indicated an increasing dispersion of C_{16}2MeB–RCM–NH_3 nanosheets compared to that of C_{16}2MeB–Mnt. The organic cations in Mnt influenced the absolute value, which decreases in the order of 2EtOH2Me (3.61) > C_{16}2MeB (3.68) > $2C_{18=}$2Me–Mnt (3.82). C_{16}2MeB–RCM–NH_3 (CEC = 0.52 meq g^{-1}) may form nanosheet aggregates with a moderate size, improving the thermal insulation performance.

Small-angle X-ray scattering analysis of organo-Mnt in a premix solution

The formation mechanism of the aforementioned aggregates/exfoliated dispersion of the silicate layers has been discussed considering the PU polymerization process. As shown in Fig. 9, the SAXS patterns of C_{16}2MeB–Mnt (CEC = 1.19 meq g^{-1}), C_{16}2MeB–RCM–NH_3 (CEC = 0.52 meq g^{-1}), and C_{16}2MeB–RCM (CEC = 0.29 meq g^{-1}) were recorded after mixing the premix solution prior to the polymerization. The aim was to compare the structural changes (*i.e.*, intercalation, delamination, and exfoliation) by immersing PO (Fig. 5), subsequent mixing with the premix solution, and final cross-linking with isocyanate to form PU foams (Fig. 8A). The power law relationship, $I(q) \propto q^{-3}$, in a small-angle range ($0.06 < q < 0.2$ nm^{-1}) indicated a mixed and complicated phase rather than a two-dimensional anisotropic liquid crystalline phase.[62] According to the SR-SAXS results shown in Fig. 8, lamellar structures with d = 4.5 nm would reform in C_{16}2MeB–Mnt (CEC = 1.19 meq g^{-1}) during the cross-linking with isocyanate owing to the high layer charge density. As illustrated in Fig. 10A, the water molecules in the premix solution would expand the interlayer space to disperse the silicate layers, irrespective of the difference in the layer charge density. Isocyanate hydrolysis consumes water, leading to restacking/dense ordering by losing compatibility

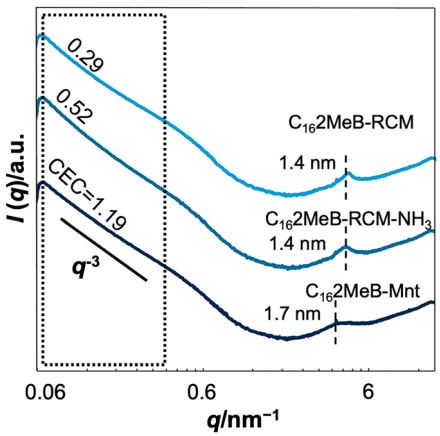

Fig. 9 SAXS patterns of mixtures of the premix solution with C_{16}2MeB-modified montmorillonite samples prepared using different layer charge densities.

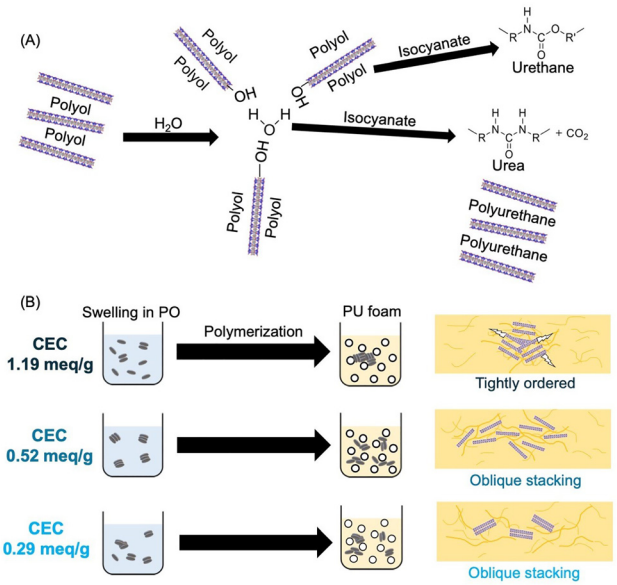

Fig. 10 (A) Schematic drawings of the change in the dispersibility of the silicate layers when (A) water molecules in the premix solution reacted and (B) the polymerization was terminated.

with the PU matrix with the aid of the strong electrostatic interactions in C_{16}2MeB–Mnt (CEC = 1.19 meq g^{-1}).

Finally, the effect of the organic cations in Mnt (CEC = 1.19 meq g^{-1}) is discussed in terms of the compatibility with which kind of molecular aggregates (urethane, urea, or isocyanurate groups) is favored, in the polymeric main skeleton formed *via* cross-linking. Through the low affinity of 2EtOH2Me with PO, a high dispersion of 2EtOH2Me–Mnt in the PU foams was obtained, even at a high CEC. Owing to the high polarity of 2EtOH2Me, the silicate layer was dispersed in a more polar domain (urea aggregate) through possible reactions of isocyanate with hydroxyl groups in 2EtOH2Me.[63] If the contribution of a dense polyurea domain to gas permeation is negligible, the dispersion of 2EtOH2Me–Mnt would have a neutral effect on the thermal insulation performance. For C_{16}2MeB–Mnt, a little improvement in the thermal insulation would result from a dense ordering, as described above, rather than dispersing *via* possible interactions of C_{16}2MeB (*e.g.*, aromatic ring) with the PU domain. For $2C_{18=}$2Me–Mnt, a negative effect on the insulation performance was observed, despite its high affinity with PO. The bulkiness and flexibility of $2C_{18=}$2Me derived from the *gauche* conformation with a lower packing formed a microscopic porous structure, possibly lowering the effects on sealing insulation gases.

Despite the low affinity of PO with C_{16}2MeB–RCM–NH_3 (CEC = 0.52 meq g^{-1}) and C_{16}2MeB–RCM (CEC = 0.29 meq g^{-1}), a suitable dispersion was obtained in the PU foams for good insulation. According to the discussion using the slope of the power law relationship (Fig. 8, left), the C_{16}2MeB-modified nanosheets were a consequence of restricting the dense ordering by weak electrostatic interactions. This ordering structure can be illustrated as an "oblique stacking" in the PU matrix (Fig. 10B) for the slow diffusion of insulation gases. A high aspect ratio of a nanosheet from huge crystals[64] led to superior gas-barrier properties.[65] In the present

system, gentle stacking (oblique stacking) was effective in improving the gas barrier in the thin wall of the PU foam. This was accomplished by tuning the CEC of the submicrometer-scaled nanosheets.

Effects of Mnt on reducing CO_2 emissions in a detached house model

The resulting PU foam hybridized with C_{16}2MeB–RCM–NH_3 exhibited a good thermal insulation performance. Here, the insulation performance was used to simulate the influence of reducing power consumption in heating in a typical detached house located in a cold region in Japan. Considering that the lifespan of a house is several tens of years, the simulation was accumulated over 30 years. As a result of simulating the time-course increase in the thermal conductivity (Fig. S4), the thermal conductivity for the C_{16}2MeB–RCM–NH_3-containing PU converged to 23.8 mW m^{-1} K^{-1}, which was smaller than that of the Mnt-free PU foam (24.2 mW m^{-1} K^{-1}) at 120 days. A simulation[66] also afforded differences in the thermal conductivity at 30 years of 27.3 and 27.6 mW m^{-1} K^{-1}, when C_{16}2MeB–RCM–NH_3 is present and absent, respectively. The differences in thermal conductivity are responsible for heat transfer from the interior to the outside. Thus, the specific heat losses were calculated to be 0.55 and 0.56 W m^{-2} K^{-1} for the C_{16}2MeB–RCM–NH_3-containing PU and Mnt-free PU foams, respectively. According to the specific heat loss, the 1-year power consumption within a heating period (from October 24 to May 1 in Nagano City) was observed to decrease from 5546 to 5505 kWh by the addition of C_{16}2MeB–RCM–NH_3 to PU foam. Consequently, 570 kg-CO_2 of the total CO_2 emission in heating over 30 years can be reduced, according to the difference in multiplying the CO_2 emission coefficient (0.459 kg-CO_2 $(kWh)^{-1}$) with the thirty-fold power consumption.

Conclusions

The dispersion characteristics of clay nanosheets (silicate layers of Mnt) in PU foam were investigated to direct the rational design of a thermal insulation gas-barrier agent in thin PU walls. The degree of ordering of clay nanosheets in the polymeric matrix was diminished using the polar organic cation, 2EtOH2Me. However, a neutral effect was obtained upon improving the thermal insulation probably because of interactions with the polyurea matrix. The interlayer modification of Mnt with C_{16}2MeB with a moderate layer charge density afforded a suitable gas-barrier agent in the PU foam because a reduction in the layer charge density prevented the formation of densely ordered stacking. The C_{16}2MeB-modified Mnt contributed to a reduction in power consumption in heating (or CO_2 emission) owing to the simulation of heat transfer from the inner detached house model to the outer atmosphere.

Author contributions

Tomonori Wanatabe and Haruna Sasaki: original draft preparation, investigation, methodology, data analysis, and writing – review and editing. Yuhei Nakashima: investigation, methodology and data analysis. Kunihiro Kitano: data analysis for SAXS. Nobuyoshi Miyamoto: data analysis for SAXS and review. Hideki Takamura: calculation and data analysis for reducing CO_2 emission. Tomohiko Okada: conceptualization, writing – review and editing, and supervision.

Conflicts of interest

There are no conflicts to declare.

Data availability

The data supporting the findings of this study are available from the corresponding author, T. O., upon reasonable request.

Supplementary information: Chemical composition of the premix solution, schematic drawing of a typical wooden two-storey detached house (Fig. S1), TG–DTA curves of organo-Mnts (Fig. S2 and S3), calculation of standard reaction Gibbs energy for reaction between ammonium and Li^+ fixed into Mnt, time-course profiles of the thermal conductivity of the clay-loaded PU foams (Fig. S4), and SEM image of a PU foam (Fig. S5). See DOI: https://doi.org/10.1039/d5ma00651a.

Acknowledgements

This work was supported by JSPS KAKENHI (Grant-in-Aid for Scientific Research), grant number of 24K08057. We also acknowledge Prof. Makoto Ogawa and Dr Kamonnart Imwiset (VISTEC) for performing synchrotron radiation X-ray diffraction experiments at BL19B2, SPring-8, with approval from the Japan Synchrotron-Radiation Research Institute (JASRI) (program number 2023B1802) under the direction of Dr Keiichi Osaka (JASRI). The calculation of the CO_2 emission was kindly contributed by Mr Yuki Yoshida (Takamura Laboratory, Shinshu University).

Notes and references

1 C. Yang, L. Fischer, S. Maranda and J. Worlitschek, *Energy Build.*, 2015, **87**, 25.
2 C. Ligoure, M. Cloitre, C. Le Chatelier, F. Monti and L. Leibler, *Polymer*, 2005, **46**, 6402.
3 X. D. Zhang, C. W. Macosko, H. T. Davis and A. D. Nikolov, *J. Colloid Interface Sci.*, 1999, **215**, 270.
4 A. Fraleoni-Morgera and M. Chhikara, *Adv. Eng. Mater.*, 2019, **21**, 1801162.
5 S. Perez-Tamarit, E. Solorzano, R. Mokso and M. A. Rodriguez-Perez, *Polymer*, 2019, **166**, 50.
6 P. Cimavilla-Roman, S. Perez-Tamarit, M. Santiago-Calvo and M. Rodriguez-Perez, *Eur. Polym. J.*, 2020, **135**, 109884.
7 S. Czlonka, A. Strakowska, K. Strzelec, A. Kairyte and S. Vaitkus, *Polym. Test.*, 2019, **75**, 12.
8 C. H. Dan, M. H. Lee, Y. D. Kim, B. H. Min and J. H. Kim, *Polymer*, 2006, **47**, 6718.

9 S. Estravis, J. Tirado-Mediavilla, M. Santiago-Calvo, J. Luis Ruiz-Herrero, F. Villafane and M. Rodriguez-Perez, *Eur. Polym. J.*, 2016, **80**, 1.
10 M. Stanzione, M. Oliviero, M. Cocca, M. E. Errico, G. Gentile, M. Avella, M. Lavorgna, G. G. Buonocore and L. Verdolotti, *Carbohydr. Polym.*, 2020, **231**, 115772.
11 H. Haridevan, M. S. McLaggan, D. A. C. Evans, D. J. Martin, T. Seaby, Z. Y. Zhang and P. K. Annamalai, *ACS Appl. Polym. Mater.*, 2021, **3**, 3528.
12 A. Kairyte, O. Kizinievic, V. Kizinievic and A. Kremensas, *Composites, Part A*, 2019, **117**, 193.
13 C. Forest, P. Chaumont, P. Cassagnau, B. Swoboda and P. Sonntag, *Prog. Polym.*, 2015, **41**, 122.
14 M. Joshi, B. Adak and B. S. Butola, *Prog. Mater. Sci.*, 2018, **97**, 230.
15 G. Choudalakis and A. D. Gotsis, *Eur. Polym. J.*, 2009, **45**, 967.
16 C. Wolf, H. Angellier-Coussy, N. Gontard, F. Doghieri and V. Guillard, *J. Membr. Sci.*, 2018, **556**, 393.
17 Y. Fukushima and S. Inagaki, *J. Inclusion Phenom.*, 1987, **5**, 473.
18 A. Usuki, Y. Kojima, M. Kawasumi, A. Okada, Y. Fukushima, T. Kurauchi and O. Kamigaito, *J. Mater. Res.*, 1993, **8**, 1179.
19 A. Okada and A. Usuki, *Macromol. Mater. Eng.*, 2006, **291**, 1449.
20 *Handbook of Clay Science (Developments in Clay Science, Vol. 1)*, ed. F. Bergaya, B. K. G. Theng and G. Lagaly, Elsevier, Amsterdam, 2006.
21 T. K. Chen, Y. I. Tien and K. H. Wei, *Polymer*, 2000, **41**, 1345.
22 M. Alexandre and P. Dubois, *Mater. Sci. Eng.*, 2000, **28**, 1.
23 G. Choudalakis and A. D. Gotsis, *Curr. Opin. Colloid Interface Sci.*, 2012, **17**, 132.
24 A. Akelah, A. Rehab, T. Agag and M. Betiha, *J. Appl. Polym. Sci.*, 2007, **103**, 3739.
25 A. Decarreau, O. Graudy and S. Petit, *Appl. Clay Sci.*, 1992, **7**, 147.
26 K. Saito, M. Morita, T. Okada, R. Wijitwongwan and M. Ogawa, *Chem. Soc. Rev.*, 2024, **53**, 10523.
27 G. Lagaly, *Clay Miner.*, 1981, **16**, 1.
28 T. Okada, Y. Seki and M. Ogawa, *J. Nanosci. Nanotechnol.*, 2014, **14**, 2135.
29 S. Minase, *J. Oleo Sci.*, 2014, **14**, 205.
30 T. Hayakawa, M. Minase, K. Fujita and M. Ogawa, *Clays Clay Miner.*, 2016, **64**, 275.
31 T. J. Pinnavaia and G. W. Beall, *Polymer-Clay Nanocomposites*, John Wiley & Sons Ltd, New York, 2001.
32 S. S. Ray and M. Okamoto, *Prog. Polym. Sci.*, 2003, **28**, 1539.
33 U. Hofmann and R. Klemen, *Z. Anorg. Allg. Chem.*, 1950, **262**, 95.
34 W. F. Jaynes and S. A. Boyd, *Clays Clay Miner.*, 1991, **39**, 428.
35 R. L. Zhu, L. Z. Zhu and L. H. Xu, *Colloids Surf., A*, 2007, **294**, 221.
36 P. Komadel, J. Madejová and J. Bujdák, *Clays Clay Miner.*, 2005, **53**, 313.
37 C. C. Su and Y. H. Shen, *Colloids Surf., A*, 2005, **259**, 173.
38 R. L. Zhu, J. B. Zhao, F. Ge, L. F. Zhu, J. X. Zhu, Q. Tao and H. P. He, *Appl. Clay Sci.*, 2014, **88–89**, 73.
39 J. Bujdák, *J. Phys. Chem. C*, 2015, **119**, 12016.
40 T. Ebina, *Chem. Rec.*, 2018, **18**, 1020.
41 P. R. Bodart, L. Delmotte, S. Rigolet, J. Brendle and R. D. Gougeon, *Appl. Clay Sci.*, 2018, **157**, 204.
42 M. Kubota and K. Kurosaka, *Jp. Pat.*, 6288764, 2018.
43 K. Hara and M. Kubota, *Jp. Pat.*, 7368842, 2023.
44 M. Ogawa, T. Aono, K. Kuroda and C. Kato, *Langmuir*, 1993, **9**, 1529.
45 M. Ogawa, T. Matsutomo and T. Okada, *J. Ceram. Soc. Jpn.*, 2008, **116**, 1309.
46 T. Okada, T. Matsutomo and M. Ogawa, *J. Phys. Chem. C*, 2010, **114**, 539.
47 Z. Navrátilová and M. Mucha, *J. Solid State Electrochem.*, 2015, **19**, 2013.
48 M. Majdan, E. Sabah, M. Bujacka, S. Pikus and A.-G. Plaska, *J. Mol. Struct.*, 2009, **938**, 29.
49 K. J. Imwiset, T. Hayakawa, Y. Fukushima, T. Yamada and M. Ogawa, *Langmuir*, 2019, **35**, 13977.
50 G. Lagaly and K. Beneke, *Colloid Polym. Sci.*, 1991, **269**, 1198.
51 G. Lagaly, *Solid State Ionics*, 1986, **22**, 43.
52 L. Mercier and C. Detellier, *Clays Clay Miner.*, 1994, **42**, 71.
53 L. L. Zhong, S. X. Hu, X. J. Yang, M. Yang, T. T. Zhang, L. C. Chen, Y. L. Zhao and S. X. Song, *Colloids Surf., A*, 2021, **617**, 126364.
54 E. N. Skoubris, G. D. Chryssikos, G. E. Christidis and V. Gionis, *Clays Clay Miner.*, 2013, **61**, 83.
55 T. Ebina and F. Mizukami, *Adv. Mater.*, 2007, **19**, 2450.
56 T. Lan and T. J. Pinnavaia, *Chem. Mater.*, 1994, **6**, 2216.
57 R. Kato, A. Kakugo, K. Shikinaka, Y. Ohsedo, A. Kabir and N. Miyamoto, *ACS Omega*, 2018, **3**, 14869.
58 D. Yamaguchi, N. Miyamoto, K. Satoshi, T. Nakato and T. Hashimoto, *J. Appl. Crystallogr.*, 2007, **40**, s101.
59 K. Kim, J. Kim and I. Chung, *J. Appl. Polym.*, 2011, **119**, 1287.
60 N. Miyamoto, R. Kawai, K. Kuroda and M. Ogawa, *Appl. Clay Sci.*, 2000, **16**, 161.
61 T. Okada, K. Izumi, S. Kawaguchi, C. Moriyoshi, T. Fujimura, R. Sasai and M. Ogawa, *Langmuir*, 2021, **37**, 10469.
62 T. Morooka, Y. Ohsedo, R. Kato and N. Miyamoto, *Mater. Adv.*, 2021, **2**, 1035.
63 Z. Zu, Z. W.-W. Kong, M.-X. Zhou and M. Peng, *Chin. J. Polym. Sci.*, 2010, **28**, 615.
64 M. Stöter, D. A. Kunz, M. Schmidt, D. Hirsemann, H. Kalo, B. Putz, J. Senker and J. Breu, *Langmuir*, 2013, **29**, 1280.
65 M. Röhrl, R. L. Timmins, S. Rosenfeldt, D. D. Schuchardt, F. Uhlig, S. Nürmberger and J. Breu, *ACS Appl. Mater. Interfaces*, 2023, **15**, 22524.
66 Y. Nakashima, *TOSOH Res. Technol. Rev.*, 2019, **63**, 37.